Available online at www.sciencedirect.com
ScienceDirect
Ceramics International 36 (2010) 863–870
CERAMICS INTERNATIONAL
www.elsevier.com/locate/ceramint

# Fabrication of rigid media tube filter bound with aluminum borate using $Al_2O_3$–$B_2O_3$–MgO frit for filtration of molten aluminum

Osamu Yamakawa [a,1], Hiroshi Shirakawa [b,2], Minoru Hashiba [c,3], Osamu Sakurada [c,*]

[a] NGK ADREC Co., Ltd., 3040 Mizano, Mitake-cho, Kani-gun, Gifu 505-0112, Japan
[b] NGK INSULATORS, Ltd., 2-56 Suda-cho, Mizuho-ku, Nagoya, Aichi 467-8530, Japan
[c] Gifu University, 1-1 Yanagido, Gifu 501-1193, Japan

Received 21 August 2009; received in revised form 26 August 2009; accepted 23 September 2009
Available online 29 October 2009

**Abstract**

We performed a study of a tube filter binding agent for molten aluminum (rigid media tube filter, RMF). In this study, we examined the formation mechanism of aluminum borate ($9Al_2O_3{\cdot}2B_2O_3$; 9A2B) from $Al_2O_3$–$B_2O_3$–MgO frit composition, which used MgO instead of CaO in the $Al_2O_3$–$B_2O_3$–CaO frit in our previous report. The results indicated that crystallization of 9A2B is easier in $Al_2O_3$–$B_2O_3$–MgO compared to $Al_2O_3$–$B_2O_3$–CaO, in that crystals are formed with only a heating process, and the amount of crystallization increases depending on the calcination temperature and the heat load over the retention time. A tube filter made of $Al_2O_3$–$B_2O_3$–MgO frit contained a larger amount of 9A2B crystals and therefore its strength did not deteriorate until a very high temperature of 1200 °C was reached, and its coefficient of thermal expansion was low. This is an advantageous property for RMF used under constraints and high temperatures. In addition, when the amount of 9A2B crystal formation increases, the wettability of molten aluminum decreases, and it becomes more difficult for molten aluminum to impregnate the filter material, but we found that corrosion resistance was high.


*Keywords:* Aluminum borate; $9Al_2O_3{\cdot}2B_2O_3$; Rigid media tube filter; RMF

## 1. Introduction

As metallic aluminum requires very small amounts of energy during regeneration (approximately 3% of that required for aluminum ingots [1]), it is considered a material with large energy-saving effect. In Japan, the recycling rate for aluminum beverage cans exceeds 90% and the overall reproduction rate for aluminum cans is approximately 60%, which is expected to increase in the future [2]. There is also a need to increase the quality of molten aluminum due to increasing demand for thin aluminum materials for cans. The admixing of foreign material during the recycling of aluminum is very likely, and thus processing of molten metal to remove foreign material is becoming increasingly important. Use of a tube filter composed of a special inorganic coarse-grained ceramic binding material is the most reliable molten metal processing technology for removal of foreign material, and is capable of removing even small-sized particles of foreign material [3]. Nowak proposed a filter for molten aluminum using sintered $Al_2O_3$ as a coarse-grained ceramic raw material, and a three-component frit, $Al_2O_3$–$B_2O_3$–CaO, as an inorganic binding material [4]. Ihara et al. [5] confirmed that $9Al_2O_3{\cdot}2B_2O_3$ (referred to hereafter as 9A2B) crystals were formed from a wide range of compositions comprised of the three components, $Al_2O_3$–$B_2O_3$–CaO. We found that 9A2B crystals are not formed from the three-component frit ($Al_2O_3$–$B_2O_3$–CaO) alone, but that 9A2B crystal formation requires raw material of $Al_2O_3$ [6]. In addition, we reported that $Al_2O_3$ filter material coated with 9A2B crystals has a small coefficient of thermal expansion (0.57% at 1000 °C), and maintained strength over 6 MPa at a high temperature of 1200 °C, is difficult to wet with molten aluminum, and has marked corrosion resistance. However, the level of 9A2B crystal production was low, and the strength deteriorates at temperatures exceeding 1000 °C as the binding

* Corresponding author. Tel.: +81 58 293 2574; fax: +81 58 293 2794.
*E-mail addresses:* yamakawa@ngk-adrec.co.jp (O. Yamakawa), heros@ngk-adrec.co.jp (H. Shirakawa), hashiba@apchem.gifu-u.ac.jp (M. Hashiba), sakurada@gifu-u.ac.jp (O. Sakurada).
[1] Tel.: +81 574 67 3410; fax: +81 574 67 1465.
[2] Tel.: +81 52 872 7721; fax: +81 52 872 7743.
[3] Tel.: +81 58 293 2574; fax: +81 58 293 2794.

0272-8842/$36.00 
doi:10.1016/j.ceramint.2009.09.033

agent composition has a large glass content, and elution of calcium in the aluminum–magnesium alloy melt became an issue [6].

On the other hand, Ray reported that when 9A2B crystals are formed from $Al_2O_3$ and $B_2O_3$, adding CaO, $CaAl_2B_2O_7$ and MgO allows 9A2B to be formed at a lower temperature [7]. In this study, we replaced CaO in $Al_2O_3$–$B_2O_3$–CaO frit used by Nowak with MgO, and examined the configuration and calcination conditions of 9A2B crystals formed from $Al_2O_3$–$B_2O_3$–MgO frit, as well as the suitability of $Al_2O_3$–$B_2O_3$–MgO frit as a filter material for molten aluminum.

## 2. Experimental method

### 2.1. Raw materials used

To prepare a three-component frit of $Al_2O_3$–$B_2O_3$–MgO, the same materials described in the previous report [6] were used as raw materials for $Al_2O_3$ and $B_2O_3$, and magnesium oxide (#500; Tateho Chemical Industries Co., Ltd.) was used for a raw material for Mg. The same samples as described in the previous report [6] were used as $Al_2O_3$–$B_2O_3$–CaO frit. The sintered $Al_2O_3$ coarse-grained raw material was also the same as described previously [6]. Aluminum–magnesium alloy JIS 5056 was used to assess reactivity with molten aluminum.

### 2.2. Sample preparation

The chemical composition of the $Al_2O_3$–$B_2O_3$–CaO frit used by Nowak was 35 mass% $Al_2O_3$, 40 mass% $B_2O_3$, and 25 mass% CaO [4]. In the present study, we replaced 25 mass% CaO in the frit composition used by Nowak [4] with 25 mass% MgO. To prepare frit with this composition, the prepared starting material was placed into a 99.5 mass% $Al_2O_3$ porcelain crucible and heated in an electric furnace. After melting has been confirmed, it was left in the furnace for 15 min and then quickly cooled. It was then dried at 100 °C for 24 h, and dry ground to a particle size smaller than 149 μm with a ball mill. The chemical composition of this frit is shown in Table 1.

To the powder sample made with the coarse-grained raw material and frit (chemical composition shown in Table 1) mixed in a mass ratio of 85:15, was added 0.5 mass% dextrin and 6 mass% water as an organic binder, and blended using a mixer (SS-501; Kanto Kongouki Industrial Co., Ltd.). After maturation for 1 day, a mold was used, and a pressure of 10 MPa was applied to shape it into a sample piece measuring 140 mm × 30 mm × 20 mm. After air-drying for 12 h, it was dried in a drying oven (100 °C) for 12 h. The obtained sample piece was put inside an $Al_2O_3$ saggar and encapsulated in a hollow sphere of electrofused alumina material (Bubble Morundum BW, particle diameter 5–3 mm; Showa Denko K.K., Japan), which was then calcined in an electric furnace in air. The furnace was heated at a rate of 50 °C $h^{-1}$ and the temperature was kept at the maximum temperature for 1 h, 3 h, 5 h, and 10 h, and then cooled. Details are provided in Section 3.1. Calcination of the sample using $Al_2O_3$–$B_2O_3$–CaO frit was performed with heating at 50 °C $h^{-1}$ as described previously [6], and was kept at the maximum temperature of 1200 °C for 5 h before cooling to room temperature at a rate of 50 °C $h^{-1}$. The samples using $Al_2O_3$–$B_2O_3$–MgO frit and $Al_2O_3$–$B_2O_3$–CaO frit are referred to as sample A and sample B in this paper.

Table 1
Chemical compositions of frit for sample A and sintered alumina as coarse-grained material (mass%).

| | Frit for sample A | Sintered alumina |
|---|---|---|
| $Al_2O_3$ | 35.3 | 99.7 |
| $B_2O_3$ | 39.1 | – |
| MgO | 24.5 | – |
| $SiO_2$ | 0.6 | 0.1 |
| CaO | 0.2 | – |
| $Na_2O$ | 0.1 | 0.1 |

### 2.3. Evaluation of crystalline phase and crystallization temperature

An X-ray diffractometer (XRD) (RINT X-ray Diffractometer; Rigaku) was used for formation phase identification at room temperature, and high-temperature XRD (MXP18; MAC Science Co., Ltd.) was used for identification of formation phase during the heating and cooling processes. A Scanning Electron Microscope (SEM) (JSM-5600; JEOL Ltd.) with Energy Dispersive X-ray Spectroscopy (EDS) (JED-2140; JEOL Ltd.) and Electron Probe Micro-Analyzer (EPMA) (JXA-8800; JEOL Ltd.) were used for structural investigation.

### 2.4. Measurement of coefficient of thermal expansion and strength

The coefficient of thermal expansion was measured by cutting out a sample measuring 50 mm × 10 mm × 10 mm, and heating it from room temperature to 1000 °C at 5 °C $min^{-1}$ using a thermal dilatometer (DL-7000YH; Ulvac-Riko, Inc.). Bending strength was measured using a 3-point bending method at both room temperature and at a high temperature up to 1200 °C. Measurements were taken at room temperature using Autograph (AGS-500A; Shimadzu Co.), and those at high temperature were taken using a custom-built apparatus for bending strength measurement at high temperature.

### 2.5. Reactivity assessment with molten aluminum

In assessment of the reactivity of samples with molten aluminum, we evaluated the impregnation ability and corrosion resistance. The impregnation test was conducted using the component dissolution method as described previously [6], and the impregnation rate for aluminum was determined from the apparent porosity of the sample before and after the test, according to JIS R2025 [8].

The method used for corrosion resistance evaluation was also the same as that described in the previous report, using a custom-built dynamic corrosion apparatus operated for 100 h. After cooling, the sample was taken out, and the cut and polished surface examined for structural investigation using SEM,

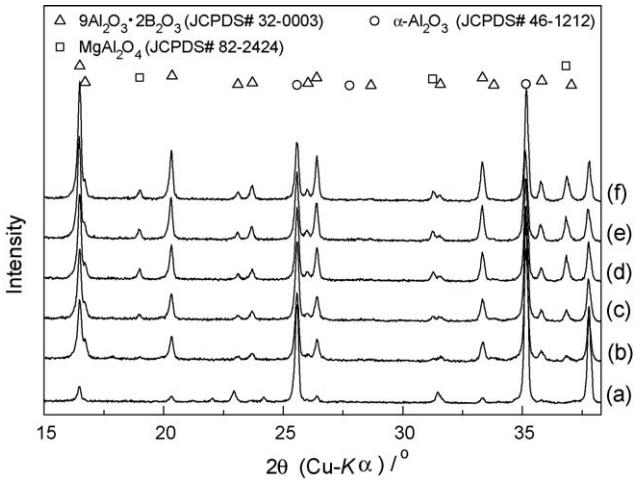


Fig. 1. X-ray diffraction patterns of sample A fired at (b) 1200 °C, (c) 1250 °C, (d) 1300 °C, (e) 1350 °C, or (f) 1400 °C for 5 h and sample B fired at 1200 °C for 5 h (a) for comparison.

comparing the thickness of binding agent before and after use. In addition, aluminum from the sample after anticorrosion test was removed with hydrochloric acid treatment, and bending strength was measured using a 3-point bending method at 750 °C.

## 3. Results and discussion

### *3.1. Effects of calcination conditions on 9A2B crystal formation*

To investigate the impact of calcination temperature of sample A made with $Al_2O_3$–$B_2O_3$–MgO frit on 9A2B crystallization, sample A was heated at 1200 °C, 1250 °C, 1300 °C, 1350 °C, and 1400 °C for 5 h and then cooled at a rate of 50 °C $h^{-1}$. For comparison, XRD measurements of sample B made with $Al_2O_3$–$B_2O_3$–CaO frit were taken after heating at 1200 °C for 5 h. The results are shown in Fig. 1. The peak height at $2\theta = 16.494°$ of 9A2B crystal from sample A calcined at 1200 °C (JCPDS No. 32-0003) was higher than that of 9A2B crystal from sample B calcined at the same temperature. On the other hand, the α-$Al_2O_3$ crystalline peak at $2\theta = 35.152°$ (JCPDS No. 46-1212) was lower in sample A compared to sample B. These observations indicated that 9A2B crystals are produced more easily with MgO composition compared to CaO composition. This is likely because the $Al_2O_3$ component from the coarse-grained raw material dissolves into the frit faster in the MgO composition compared to CaO composition, as reported previously [6], and thus the reaction between the frit component and the α-$Al_2O_3$ component occurs more easily, causing an increase in the amount of 9A2B crystal produced. The 9A2B crystalline peak of sample A becomes even higher as calcination temperature increases, and therefore the increased calcination temperature promotes the dissolution of $Al_2O_3$ component increasing the amount of 9A2B crystallization. In sample B, $CaAl_2B_2O_7$ crystals were found along with 9A2B and α-$Al_2O_3$ crystals. Aside from 9A2B, in sample A, MgO, one of the frit components, reacts with α-$Al_2O_3$ in the frit component and in the coarse-grained raw material, and a peak at $2\theta = 36.850$ (JCPDS No. 21-1152) for $MgAl_2O_4$ crystal was found with calcination at 1200 °C. This peak increased with heating temperature, as seen in the 9A2B crystal. Fig. 2 shows SEM images of the microstructure of sample A heated for 5 h at different temperatures. In Fig. 2, small amounts of 9A2B needle-shaped crystals can be seen on the surface at calcination temperatures below 1250 °C, but frit was not sufficiently melted, and the frit surface has a rippled appearance. As the calcination temperature increased, frit continued to melt, and at

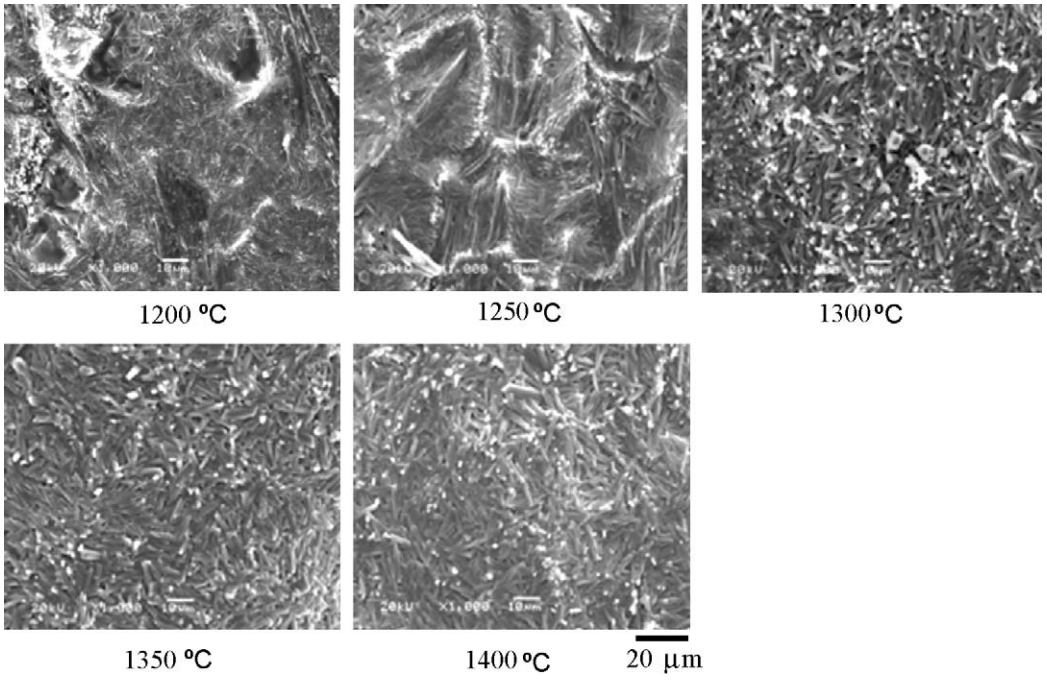


Fig. 2. SEM images of sample A fired at various temperatures for 5 h.

1300 °C, small amounts of a sphere-shaped substance that appeared to be glass were seen, but needle-shaped crystals were also seen more clearly. At temperatures above 1350 °C, the sphere-shaped substance was absent, and the development of thin and long needle-shaped crystals was observed. Fig. 3 shows SEM images of a sample heated at 1350 °C for 1 h, 3 h, 5 h, and 10 h and then cooled at a rate of 50 °C $h^{-1}$ as well as a sample heated at 1350 °C for 5 h and then cooled inside the electric furnace at a rate of 10 °C $h^{-1}$. As all samples shown in Fig. 3 had a heating temperature of 1350 °C, 9A2B needle-shaped crystals were observed on the surface in all cases, but those heated for only 1 and 3 h showed thick needle-shaped crystals with a rippled frit surface. The sample heated for 5 h had a smooth surface, but that heated for 10 h showed slight rippling on the surface. This was probably because long-term heating facilitated movement of the melted frit. With regard to cooling, the sample that was cooled slowly at a rate of 10 °C $h^{-1}$ (Fig. 3(e)) showed development of long and thin 9A2B needle-shaped crystals, but the samples that were quenched inside the electric furnace at a rate of 50 °C $h^{-1}$ (Fig. 3(c)) had thick 9A2B crystals that appeared to be fused together. In a study of the mechanism of growth of 9A2B needle-shaped crystals through chemical reaction at the interface of solid and liquid phases, Narita and Iizuka reported that fusion of needle-shaped crystals occurs due to sublimation of $B_2O_3$ [9]. However, in this study, fusion was observed with quicker cooling. This is probably not because the sublimation of $B_2O_3$ was accelerated due to quenching, but because crystallization was inhibited and there was a high glass content.

Fig. 4 shows the ratio of peak height strength of 9A2B crystals and α-$Al_2O_3$ crystals obtained by XRD measurement of calcined sample A under various calcination conditions, $Int._{9A2B\_16.5}/Int._{Al_2O_3\_35.2}$, where $Int._{9A2B\_16.5}$ is the peak height of 9A2B at $2\theta = 16.494°$ and $Int._{Al_2O_3\_35.2}$ is the peak height of

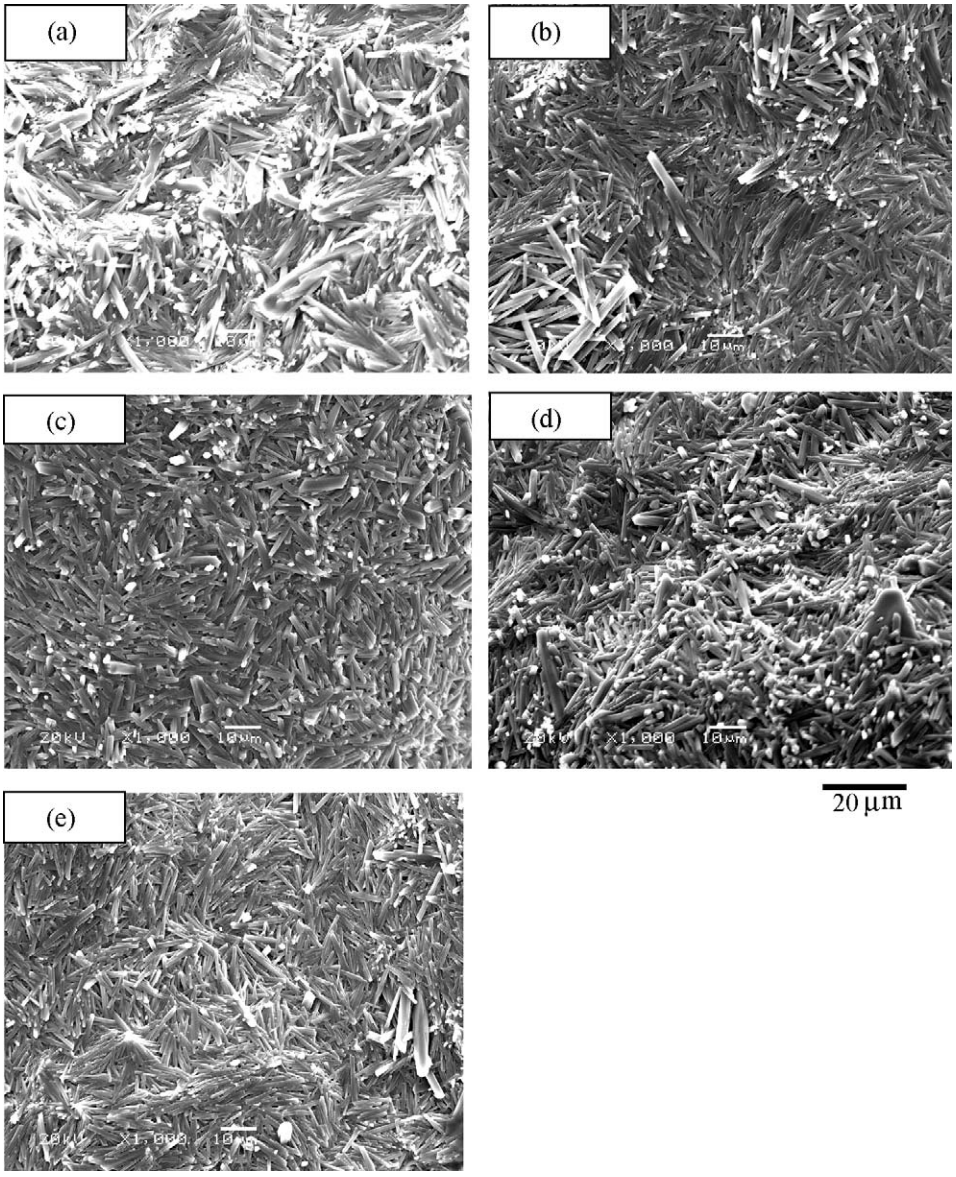


Fig. 3. SEM images of sample A fired at 1350 °C for various firing times, (a) 1 h, (b) 3 h, (c) 5 h, (d) 10 h, followed by cooling at 50 °C $h^{-1}$ and sample A fired at 1350 °C for 5 h followed by cooling at (e) 10 °C $h^{-1}$.

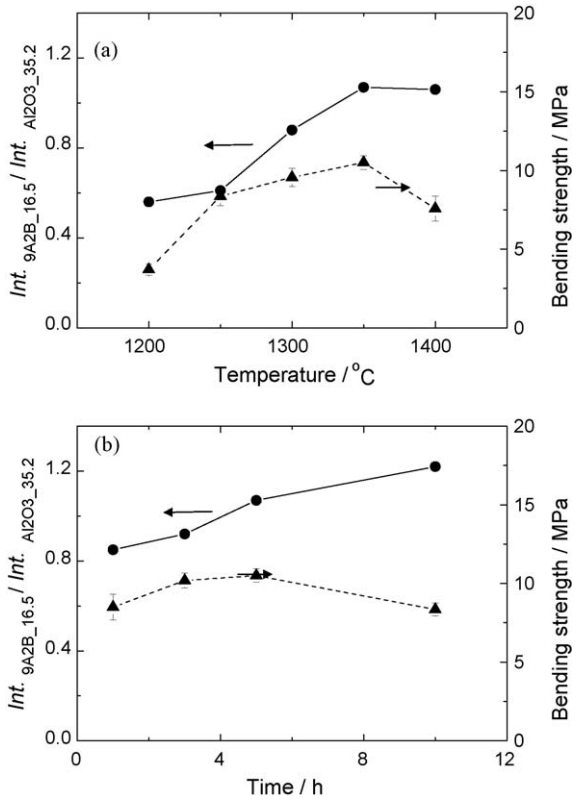


Fig. 4. Relation between ratio of peak height relative XRD intensities, $Int._{9A2B\_16.5}/Int._{Al_2O_3\_35.2}$ and bending strength of sample A fired at various firing temperatures for 5 h (a) and fired at 1350 °C for various times (b).

α-$Al_2O_3$ at $2\theta = 35.152°$, as well as the relationship with the bending strength at room temperature. Fig. 4 shows how the height strength ratio $Int._{9A2B\_16.5}/Int._{Al_2O_3\_35.2}$ increases depending on heating temperature peak and the duration of heating. $Int._{9A2B\_16.5}/Int._{Al_2O_3\_35.2}$ for calcination at 1250 °C showed a gradual increase compared to the ratio for calcination at 1200 °C, but $Int._{9A2B\_16.5}/Int._{Al_2O_3\_35.2}$ increased rapidly for calcination at higher temperatures, peaking at 1350 °C. Bending strength at room temperature increased in proportion to calcination temperature and a local maximal value of 10.5 MPa was reached at calcination temperature of 1350 °C as observed for $Int._{9A2B\_16.5}/Int._{Al_2O_3\_35.2}$. $Int._{9A2B\_16.5}/Int._{Al_2O_3\_35.2}$ also increased with increasing duration of heating. Bending strength at room temperature showed a local maximal value of 10.5 MPa when heated for 5 h, and the value decreased to 8.34 MPa on heating for 10 h. This was probably because the amount of 9A2B crystallization increased at this heat load and the strength would also increase, and therefore at heat loads exceeding this level, the viscosity of the melted frit decreased and did not contribute to the binding of coarse-grained raw materials. The lowered strength may also be due to increased volatilization volume of $B_2O_3$.

Based on the above results, we found that 9A2B crystals are produced easily from sample A using $Al_2O_3$–$B_2O_3$–MgO frit compared to sample B using $Al_2O_3$–$B_2O_3$–CaO frit. The relationship between crystallization and calcination conditions indicated that although 9A2B crystals are produced with calcination at 1200 °C, the amount produced increases at 1300 °C or higher when there is sufficient melting of the frit, and the amount of crystallization is dependent on the heat load (maximum temperature and duration). However, we found that the bending strength at room temperature was not dependent on the amount of crystallization, and was maximized when calcined at 1350 °C for 5 h. Narita and Iizuka [9] reported that calcination at a temperature of 1200–1300 °C for 3 h or more is required for 9A2B crystallization, but in a mixed system consisting of $Al_2O_3$–$B_2O_3$–MgO frit and $Al_2O_3$ coarse-grained raw material, calcination at 1350 °C for 5 h is optimal for 9A2B crystal formation and strength development, although 1300 °C is sufficient for the frit to melt. This is probably a difference in optimal formation conditions due to differences in the reaction mechanism. 9A2B needle-shaped crystals were not markedly affected by the rate of cooling, but under quenching conditions, fusion between 9A2B crystals was observed associated with lower strength.

### 3.2. Discussion of crystallization mechanism

To determine the crystallization mechanism of the $Al_2O_3$–$B_2O_3$–MgO frit, XRD measurements of a mixture of equal parts frit and calcined $Al_2O_3$ (A-37, average particle size 1.9 μm; Showa Denko K.K.) were obtained at a room temperature (30 °C) and over the heating process from 700 °C to 1300 °C, as described previously [6]. The results are shown in Fig. 5. Fig. 6 shows the XRD measurement results over the cooling process from 1300 °C. Fig. 5 indicates that crystallization of 9A2B began at 800 °C in the heating process, and the amount of crystal increased until 1200 °C. Simultaneously, the amount of α-$Al_2O_3$ decreased, and disappeared completely at 1300 °C. As the 9A2B crystals were formed, $MgAl_2O_4$ crystals were also formed, and the amount produced increased with temperature. No marked changes in the 9A2B crystalline peak height were observed in the cooling process shown in Fig. 6. In $Al_2O_3$–$B_2O_3$–CaO frit, the amount of 9A2B crystal produced increased over the cooling process, but in $Al_2O_3$–$B_2O_3$–MgO frit, 9A2B crystallization had already completed during the heating process, and mineral transformation was not observed during the cooling process. This

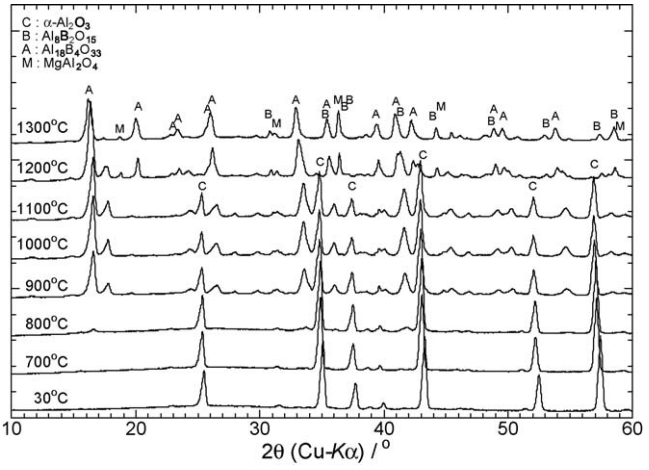


Fig. 5. XRD patterns of the mixture of $Al_2O_3$–$B_2O_3$–MgO frit and calcined alumina heated from 30 °C to 1300 °C.

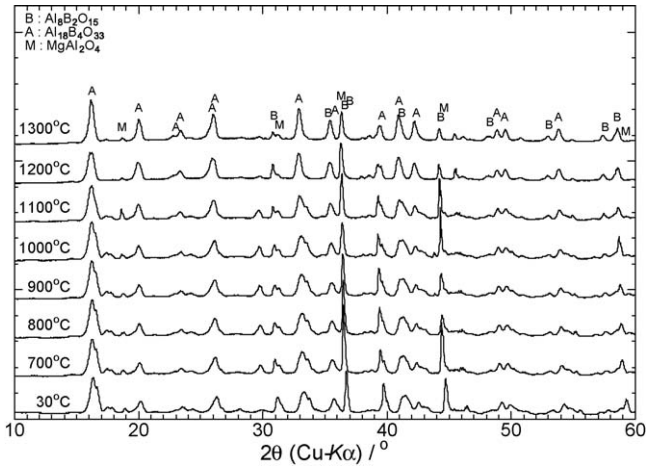


Fig. 6. XRD patterns for the mixture of $Al_2O_3$–$B_2O_3$–MgO frit and calcined alumina heated at 1300 °C followed by cooling from 1300 °C to 30 °C.

was because crystallization occurred more easily in $Al_2O_3$–$B_2O_3$–MgO frit compared to $Al_2O_3$–$B_2O_3$–CaO frit, and thus all crystallization was completed during the heating process. The amount of 9A2B crystal was expected to increase with changes in the ratio of frit to α-$Al_2O_3$ with increasing amounts of α-$Al_2O_3$. The peak for $MgAl_2O_4$ crystals was slightly higher in the cooling process, which indicated that $MgAl_2O_4$ crystals may also be formed over the cooling period.

EPMA surface analysis was performed on the binding agent of sample A calcined at 1350 °C for 5 h and then cooled at a rate of 50 °C $h^{-1}$. Fig. 7 shows the mapping results for B, Mg, Al, and Si, as well as the results of comparative analysis of the relative concentrations of each component. As shown in Fig. 7, B was present mainly on the surface layer of the binding agent, and the amount decreased progressively deeper inside the binding agent. Mg was present on the surface layer of the binding agent, and was not present in the middle layer, but was abundant in the inner layer (interface with the coarse-grained raw material). The distribution of Al was the opposite of that of Mg. Based on the distribution of each component described above, the mechanism of crystallization appears to be that 9A2B crystals are deposited on the melted frit surface, and the amount of crystallization increases with temperature, continuing until all α-$Al_2O_3$ is exhausted. On the other hand, $MgAl_2O_4$ crystals existed only on the surface layer of the binding agent, with uncrystallized $B_2O_3$ and MgO remaining in the innermost layer. As excess MgO was abundant in the innermost layer, α-$Al_2O_3$ was likely to react with $B_2O_3$ rather than with MgO,

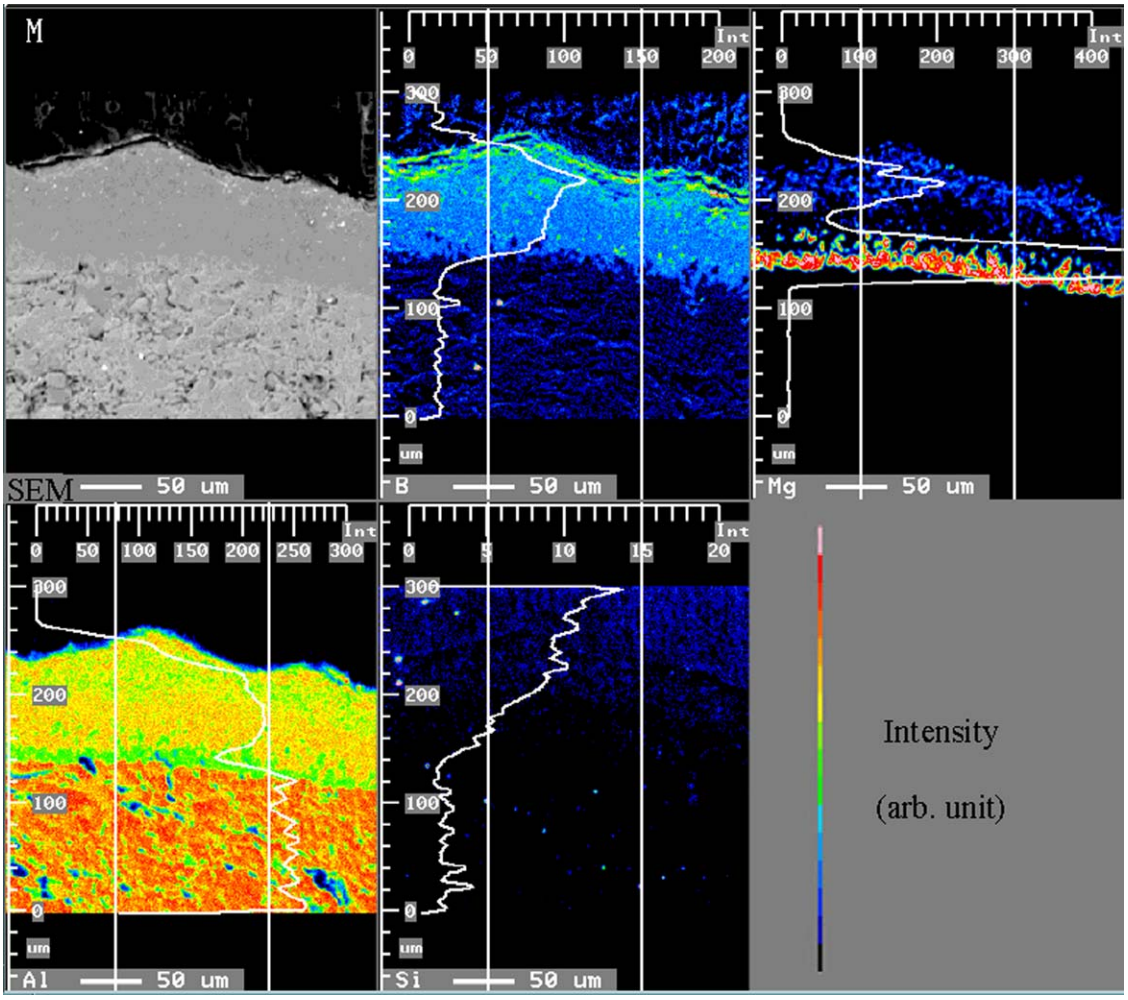


Fig. 7. EPMA mapping analysis patterns of B, Mg, Al, and Si for sample A heated at 1350 °C for 5 h.

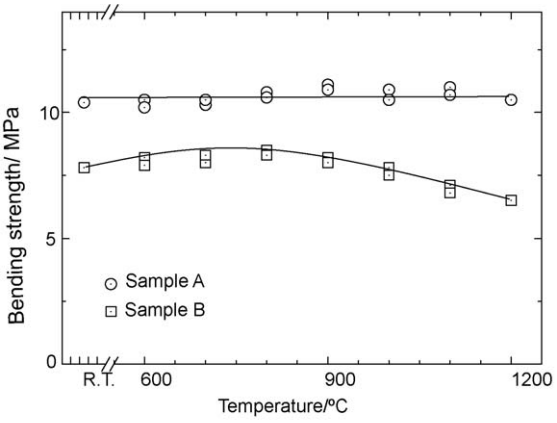


Fig. 8. Bending strength of sample A fired at 1350 °C for 5 h and sample B fired at 1200 °C for 5 h as a function of measurement temperature.

producing more 9A2B crystals compared to the case with $MgAl_2O_4$.

### 3.3. Thermal characteristics of $Al_2O_3$–$B_2O_3$–MgO frit

Fig. 8 shows the measurements of bending strength taken at different temperatures of sample A calcined at 1350 °C for 5 h and then cooled at a rate of 50 °C $h^{-1}$, and of sample B calcined at 1200 °C. Sample B maintained a bending strength of approximately 8 MPa from room temperature to 1000 °C, but the strength decreased above 1000 °C to 6 MPa at 1200 °C. The XRD measurement results shown in Fig. 1 suggest that the decrease in strength of sample B was because it had a small amount of 9A2B crystal production in the binding agent, and it also had borate glass, which has a low melting point. The bending strength of sample A was maintained between 10 MPa and 11 MPa from room temperature to 1200 °C because sample A had a higher 9A2B crystal content, which has higher melting point (above 1400 °C [9,10]), as shown in Fig. 1. Considering the operating temperature of aluminum in the field, sample B is sufficient for normal use, but sample A has stable strength to even higher temperatures and therefore has greater reliability.

Both samples A and B had linear coefficients of thermal expansion from room temperature to 1000 °C with values of 0.47% and 0.57%, respectively, at 1000 °C. The coefficient of thermal expansion of sample A was close to the thermal expansion coefficient of 9A2B ($4.2 \times 10^{-6}$ °$C^{-1}$) [7]. The coefficient of thermal expansion of sample A was small although it contained α-$Al_2O_3$, which has a large coefficient of thermal expansion. This is because the amounts of 9A2B crystal produced are large, which appears to mask the thermal expansion of α-$Al_2O_3$. As a tube filter that is used under conditions of constraint and high temperature, sample A with a small coefficient of thermal expansion and strength maintained up to a high temperature is preferable compared to sample B.

### 3.4. Reactivity test with molten aluminum

The wet-abilities of sample A (calcined at 1350 °C for 5 h then cooled at a rate of 50 °C $h^{-1}$) and sample B (calcined at 1200 °C) with molten aluminum were evaluated by measuring the impregnation time of molten aluminum into the samples. Sample B containing only a small amount of 9A2B crystal reached 100% impregnation after 22.5 h, while sample A with a high 9A2B crystal content reached only approximately 95% impregnation even after 30 h. This was because it is more difficult to wet 9A2B crystals with molten aluminum, and these observations indicated that the impregnation of molten aluminum into the sample became worse as the 9A2B crystal content in the sample increased. That is, the wettability of the sample with molten aluminum was affected by the 9A2B crystal content. When it is difficult to wet a filter medium with molten aluminum, impregnation of molten aluminum into the filter medium when initially used in operation could be insufficient, resulting in inadequate function of filter medium for removal of inclusions and thus causing a short lifespan. Improvement of wettability is a key issue to be resolved in future studies.

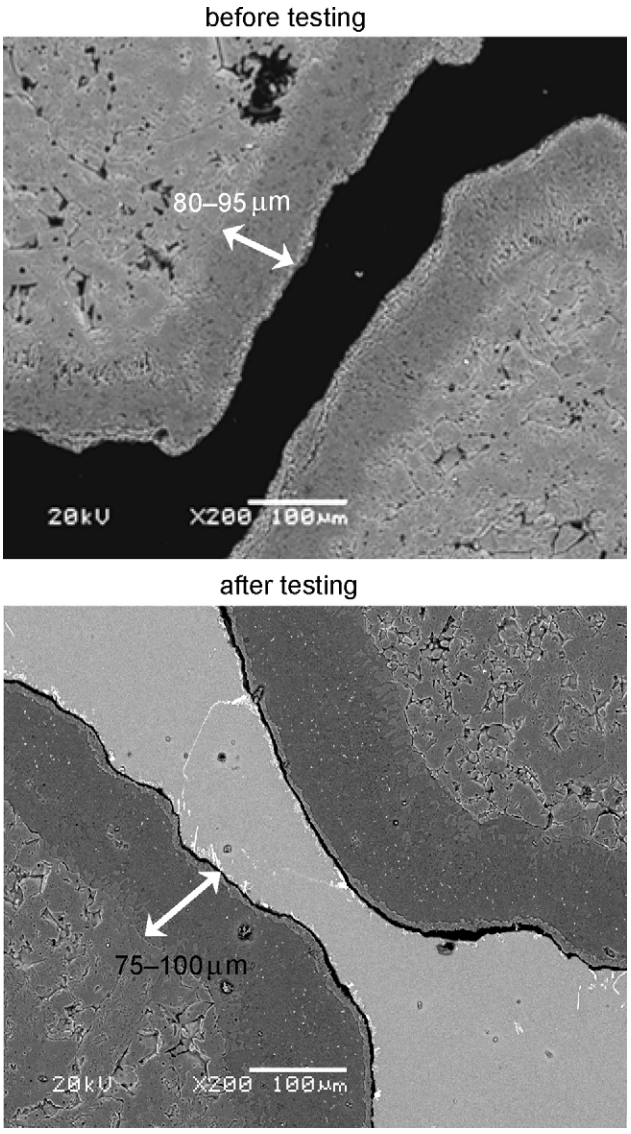


Fig. 9. SEM images of sample A before (a) and after corrosion tests (b).

Corrosion resistance was evaluated by placing sample A in JIS 5056 molten metal using the custom-built dynamic corrosion apparatus described previously [6] for 100 h. After evaluation, the sample was cut, and the polished surface subjected to structural investigation by SEM. The results shown in Fig. 9 indicate that the thickness of the binding agent of the sample was approximately the same before and after use (80–95 μm and 75–100 μm, respectively). As sample A had a high 9A2B crystal content, it had a high level of corrosion resistance against molten aluminum. After evaluation, the aluminum in the sample was removed by acid treatment, and the bending strength of the acid-treated sample was determined at 750 °C. The results showed that the bending strength after evaluation was 10.9 MPa. The bending strength before evaluation at the same temperature was 11.2 MPa, indicating that there was no significant deterioration strength. Sample A did not contain a calcium component, and therefore there was no elution of calcium component into the molten aluminum.

## 4. Conclusions

CaO in the $Al_2O_3$–$B_2O_3$–CaO three-component frit was replaced by MgO to create $Al_2O_3$–$B_2O_3$–MgO three-component frit to examine the mechanism of aluminum borate crystal formation (9A2B). The results can be summarized as follows.

(1) 9A2B crystals are more likely to be formed in $Al_2O_3$–$B_2O_3$–MgO frit compared to $Al_2O_3$–$B_2O_3$–CaO frit. The amount produced is proportional to the maximum temperature at the time of calcination and length of time kept at that temperature, but is reduced depending on quenching conditions. To obtain sufficient crystal growth and bending strength, it is effective to have a maximum temperature at the time of calcination of 1350 °C, for 5 h, followed by cooling at a rate of 50 °C $h^{-1}$.
(2) $MgO{\cdot}Al_2O_3$ crystals are also deposited at the same time 9A2B crystals are formed. However, the reactivity of $Al_2O_3$ component is higher with $B_2O_3$, and thus the formation of 9A2B has priority. $MgAl_2O_4$ crystals are only present on the surface layer of the binding agent.
(3) The sample made with $Al_2O_3$–$B_2O_3$–MgO frit did not show a reduction in strength even at high temperatures up to 1200 °C, and maintained a strength greater than 10 MPa. We also found that the coefficient of thermal expansion is as low as that of 9A2B.
(4) The sample using $Al_2O_3$–$B_2O_3$–MgO frit has a high 9A2B content, and therefore has low wettability with molten aluminum but has high corrosion resistance.

The above results indicate that $Al_2O_3$–$B_2O_3$–MgO frit is better as a molten aluminum filter medium compared to $Al_2O_3$–$B_2O_3$–CaO frit.

## Acknowledgment

We are grateful to Dr. Seizo Obata of Gifu Prefectural Ceramics Research Institute for his help with high temperature XRD measurements.

## References

[1] K. Oosumi, Y. Nagakura, R. Masuda, Kobe Steel Engineering Reports 51 (2001) 54–57.
[2] Japan Aluminum Can Recycling Association's Annual Report, 2006.
[3] M. Otaki, Journal of Japan Institute of Light Metals (Keikinzoku) 58 (2008) 167–178.
[4] T.A. Nowak, United States Patent No. 3,747, 765 (1973).
[5] M. Ihara, K. Imai, J. Fukunaga, N. Yoshida, Journal of the Ceramic Association of Japan 88 (1980) 77–84.
[6] O. Yamakawa, H. Shirakawa, O. Sakurada, M. Hashiba, Journal of Japan Institute of Light Metals (Keikinzoku) 59 (2009) 284–289.
[7] S.P. Ray, Journal of the American Ceramic Society 75 (1992) 2605–2609.
[8] JIS R2025, 1999.
[9] T. Narita, T. Iizuka, Journal of the Ceramic Society of Japan 106 (1998) 402–409.
[10] P.J.M. Gielisse, W.T. Foster, Nature 195 (1962) 69–70.